Experimental demonstration of multifrequency impedance matching for tailored voltage waveform plasmas

Junkang Wang, Sébastien Diné, Jean-Paul Booth, Erik Johnson

Experimental demonstration of multifrequency impedance matching for tailored voltage waveform plasmas

Junkang Wang, Sebastien Dine, Jean-Paul Booth, and Erik V. Johnson

Citation: Journal of Vacuum Science & Technology A **37**, 021303 (2019); doi: 10.1116/1.5056205
View online: https://doi.org/10.1116/1.5056205
View Table of Contents: https://avs.scitation.org/toc/jva/37/2
Published by the American Vacuum Society

Experimental demonstration of multifrequency impedance matching for tailored voltage waveform plasmas

Junkang Wang,[1] Sebastien Dine,[2] Jean-Paul Booth,[3] and Erik V. Johnson[1]
[1]*LPICM, CNRS, École Polytechnique, 91128 Palaiseau, France*
[2]*SOLAYL SAS, 91400 Orsay, France*
[3]*LPP, CNRS, École Polytechnique, UPMC Univ. Paris-sud, Sorbonne Universités, 91128 Palaiseau, France*

(Received 13 September 2018; accepted 23 January 2019; published 11 February 2019)

Driving radiofrequency capacitively coupled plasmas by multiharmonic tailored voltage waveforms (TVWs) has been shown to allow considerable control over various plasma properties for surface processing applications. However, industrial adoption of this technology would benefit from more efficient solutions to the challenge of impedance matching the radiofrequency power source to the load simultaneously at multiple harmonic frequencies. The authors report on the design and demonstration of a simple, practical multifrequency matchbox (MFMB) based on a network of LC resonant circuits. The performance of the matchbox was quantified in terms of a range of matchable impedances (when matching a single frequency at a time), as well as for the independence of each match to changes at adjacent harmonics. The effectiveness of the MFMB was demonstrated experimentally on an Ar plasma excited by a three-frequency TVW with a fundamental frequency of 13.56 MHz. Under the plasma conditions studied, the power coupling efficiency (at the generator output) was increased from less than 40% (without impedance matching) to between 80% and 99% for the different exciting frequencies.
https://doi.org/10.1116/1.5056205

I. INTRODUCTION

For the optimization of surface processing by radiofrequency capacitively coupled plasmas (RF-CCP), independent control over plasma properties (notably the fluxes of reactive radicals and ions, and the ion energy distribution) is highly desirable.[1] Various strategies have been investigated to achieve more independent control of the plasma parameters, for instance (nonharmonic), dual-frequency discharges.[2] In this situation, the high frequency source (at 27 MHz or more) principally controls the plasma density (through electron heating via the fast sheath motion), whereas the ion energy at the substrate is semi-independently controlled by the voltage amplitude of the low-frequency (typically a few MHz) source. However, this technique has limitations, including the coupling between the two frequency components (particularly the electron heating and temporal ionization dynamics) which has been identified in simulations and experiments.[3–6] Furthermore, the emission of secondary electrons may further reduce the ability to independently control ion energy and flux.[7]

More recently, tailored voltage waveform (TVW) excitation has been proposed[8,9] and has been shown to provide better decoupling. In contrast to nonharmonic dual-frequency excitation (using sources that are widely separated in frequency), TVW excitation uses a voltage waveform comprising a finite Fourier series of multiple consecutive harmonics with individually adjustable amplitudes and phases. When a plasma is driven by a nonsinusoidal waveform, an electrically asymmetric plasma response can be achieved, regardless of the reactor geometry. As a consequence, a nonzero DC self-bias (V_{DC}) can be established in a plasma discharge even if it is operated in a geometrically symmetric reactor. By tuning the phase shift between the harmonics, different types of voltage waveforms with controllable asymmetric global extrema can be produced. Continuous variation of the division of the voltage between the two electrode sheaths, and therefore of the incident ion energy, can be achieved by controlling the amplitude asymmetry, while other process parameters are influenced very little. This is referred to as the electrical asymmetry effect or more precisely the amplitude asymmetry effect (AAE).[10,11] A slope asymmetry effect (SAE) has also been identified, arising from a temporal asymmetry in the rising and falling slopes of the applied voltage waveform, even when the driven waveforms have identical global extrema.[12,13] Through this effect, radically different dynamics of the sheaths in front of each electrode can be achieved, causing spatially localized electron power absorption and independent control over the ion flux to each electrode. For a comprehensive understanding of these effects, one is referred to the extensive reviews on the subject.[14,15]

In a very short amount of time, it has been shown by several groups that TVWs can be of great interest for various steps in semiconductor processing. By making use of the AAE, one can gain deeper understanding and control over epitaxial growth,[16] thin film growth,[17–20] and plasma etching,[21,22] as well as the performance of photovoltaic devices.[23] Furthermore, it has been recently demonstrated that electrode-selective processing can be achieved using this technique. Via the SAE and using a halogenated plasma chemistry, one can independently and selectively control the etching/deposition balance of silicon thin films on each electrode in the reactor.[24] It has also been shown that TVWs can reduce the problem of discharge nonuniformity that occurs with high excitation frequency and large substrates.[25]

The deployment of TVW technology in high-power industrial applications requires a simple solution to the multifrequency impedance matching challenge that this concept creates. This is necessary to enable efficient power coupling at multiple harmonics, a task that is easily achieved for single-frequency excitation using a simple L-type matching network. However, as both the plasma impedance and the response of individual passive components are frequency dependent, a single-frequency matchbox cannot simultaneously match more than one harmonic. If the frequencies are very distant (kHz vs MHz) and/or excitation waveforms are applied to different electrodes, many engineering solutions exist. However, when the waveform consists of a group of harmonics applied to a single electrode, the impedance matching problem becomes more complicated.

Until now, this problem has been handled in two ways. The first, used in research laboratories, is to use an overdimensioned amplifier that can tolerate almost complete power reflection, as described in Ref. 17, without any impedance matching. Provided the discharge volume is small enough and the amount of coupled power is sufficient, experiments can be performed with a high number of harmonics.[26] The second solution consists of using multiple individual sources, matchboxes, and filters, one for each frequency used (as described in Ref. 11). A high-power version of this solution is commercially available, after having been demonstrated by Franek *et al.*[27] However, some design efficiencies may be gained by using a low-power arbitrary waveform generator, a single (wideband) power amplifier, and a multifrequency matchbox (MFMB) (with a single input and output) capable of achieving impedance matching at all harmonics simultaneously.

A novel design for a MFMB allowing for using a single, wideband power source is the basis of a patent application by Johnson and Booth.[28] This design is based on a classical "L-type" matching network, as depicted in Fig. 1. In such networks, a "Tune" branch is connected in series with the plasma load, and a "Load" branch is connected in parallel with the RF source. These two branches consist of capacitors or inductors, whose values are adjusted to achieve optimal power transfer, in which case, the total load (plasma + matchbox) has the same characteristic output impedance as the RF source, which is typically designed to be 50 Ω.

The MFMB design described in that patent application aims to achieve two goals: simultaneous matching of three harmonic frequencies and also independent control over matching at each frequency. To do so, rather than one or two capacitors and/or inductors in the Tune and Load branches, multiple LC resonant circuits (either parallel-connected or series-connected) with resonant frequencies close to the corresponding excitation frequencies are present as sub-branches. For each sub-branch, the impedance near its resonant frequency can therefore be varied over a wide range. Moreover, since the excitation frequencies are spaced far apart, if the response of each resonant circuit is designed to be relatively narrow, the matching at each different frequency can be adjusted with adequate independence. Recently, the performance of this design was investigated by numerical simulation, using an equivalent plasma circuit model which self-consistently calculates the electron temperature and plasma density.[29] That work predicted that effective impedance matching can be achieved for plasmas operating over a range of gas pressures and using several excitation frequencies.

In this paper, we report on the experimental demonstration of a prototype of this MFMB design. The MFMB was first characterized alone to determine its range of useful operation under ideal conditions (single-frequency operation) and to examine cross-talk between frequencies. Then, it was used to match a source producing a three-harmonic TVW excitation (fundamental frequency at 13.56 MHz) to an Ar plasma load with different gas pressures and power amplitudes, and the impedance matching efficiency was characterized.

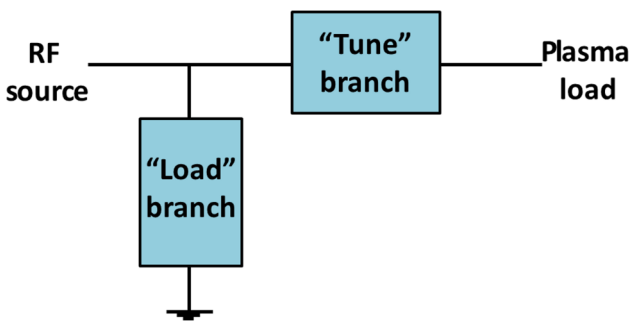

FIG. 1. Typical "L-type" matching network.

II. EXPERIMENT

A. Capacitively coupled plasma system

The experiments were carried out in a large area (0.2 m^2) capacitively coupled reactor,[30] which comprises two 500 mm diameter parallel electrodes with an interelectrode distance of 25 mm. In order to make the CCP system geometrically symmetric, a thick radial dielectric spacer ring is installed between the (grounded) side walls and the powered and grounded parallel electrodes.

The driving waveforms were produced using a system similar to that presented in detail previously in Ref. 17. The ideal voltage signal applied to the powered electrode can be expressed by

$$V(t) = V_0 \sum_{k=1}^{n} \frac{n-k+1}{n} \cos(k\omega t + \varphi), \quad (1)$$

where V_0 is the voltage amplitude prefactor, n is the number of harmonics (here set to three), ω is the angular frequency, corresponding to the fundamental frequency at 13.56 MHz, and φ is the phase shift between those harmonics. The external circuit is depicted in Fig. 2. The voltage waveform is generated by a Tektronix AFG3251 programable arbitrary waveform generator (AWG). The signal is then amplified through a PRANA AP32GN310 broadband (0.1–200 MHz) RF power amplifier, the output of which is connected to the MFMB. This type of amplifier has been used in previous studies where no MFMB was employed, as it is very tolerant to high levels of reflected power. The gain of the amplifier

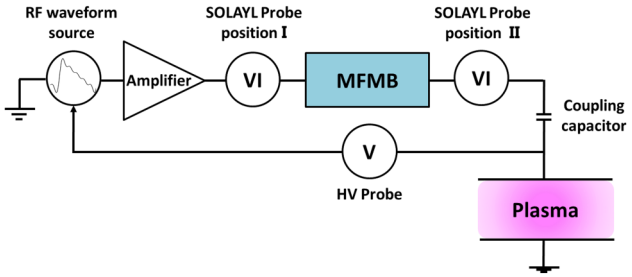

FIG. 2. Schematic of the CCP system.

cannot be adjusted, so the output voltage is determined by the input voltage amplitude. A voltage–current (VI) probe (Vigilant Power Monitor from SOLAYL SAS)[31] is installed at the input of the MFMB (SOLAYL Probe Position I) to quantify the total impedance as well as the coupled power to the total load (comprising the matching network, a coaxial coupling cable, and the plasma reactor). For certain measurements, the VI probe is installed at the output of the MFMB (but before the 6.7-m coaxial coupling cable, SOLAYL Probe Position II) to quantify the load impedance. Finally, the RF power is coupled to the reactor through a 4.5 nF capacitor to allow for the development of DC bias. Due to the frequency-dependent response of the system, the voltage waveform produced at the powered electrode usually differs in shape from the input to the amplifier. For this reason, the voltage waveform on the electrode was monitored by a high-voltage probe and digital oscilloscope. By performing a Fourier transform on the actual voltage waveform at the electrode and comparing this to the desired waveform, the signal supplied by the AWG is corrected (in amplitude and phase for each harmonic) to achieve the desired voltage waveform on the electrode.[32,33]

By using the complex load impedance Z_i measured by the VI probe at Probe Position I, one can calculate the voltage reflection coefficient at each frequency, Γ_i, using

$$\Gamma_i = \left|\frac{50 - Z_i}{50 + Z_i}\right|. \tag{2}$$

Thus, the power reflection coefficient or the coupling efficiency (as seen at the matchbox input) at the corresponding frequency k_i can also be calculated. It should be noted that this figure only considers the power that is not reflected back to the amplifier and does not distinguish between power coupled to the plasma and power absorbed in the matchbox. Measurements were carried out with an Ar plasma excited by the "peak" type TVW ($\varphi = 0$), for various gas pressures and coupled powers.

B. Impedance matching network

The electrical circuit of the MFMB used here is depicted in Fig. 3. In order to achieve matching at each frequency, the number of LC circuit sub-branches in both the "Tune" and "Load" branches must be equal to the number of excitation frequencies. In particular, parallel-connected sub-branches are used in the "Tune" branch, and series-connected sub-branches are used in the "Load" branch. This prototype MFMB was manufactured by SOLAYL SAS, and great attention was paid to the design and the placement of the various components to minimize stray impedances. The inductors are fixed air-core copper coils, and the capacitors are variable vacuum capacitors from COMET AG. The circuit is enclosed in a 19-in. rack metal box with forced air-cooling. The six capacitors can be manually tuned from outside. After rough characterization of the load impedance at the three frequencies of interest, appropriate values of the inductors and capacitors in the sub-branches were calculated. For the current design, those values are also shown in Fig. 3.

Note that it is necessary to anticipate variations in the plasma load with plasma conditions, in addition to the reactor characteristics, to choose reasonable values for these elements, as discussed in Ref. 29. In addition, since the load impedance at each frequency is not perfectly known in advance, these reactive components need to be adjustable. Preferably, the adjustable components are capacitors, as used in the current design. Finally, to design a MFMB suitable for many plasma conditions and reactors, the use of capacitors with large variable ranges is recommended.

III. CHARACTERIZATION OF THE MFMB

A. Tuning of resonant frequencies

To determine the effective range of operation of the MFMB when treated as three separate but integrated matching networks, we first examine the frequency-dependent Tune branch reactance X_{tune} for different values of capacitance in each sub-branch. To do so, for the characterization of each

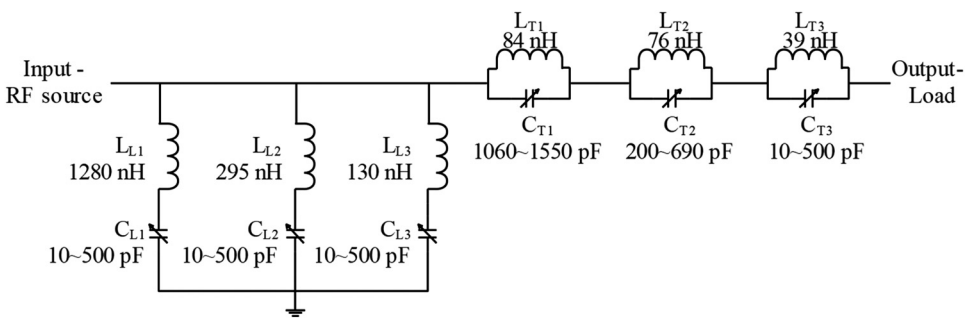

FIG. 3. Electrical network of the MFMB designed for the three-frequency TVW excited plasma.

sub-branch, the resonant frequencies of the other two sub-branches were set as far as possible away by setting the corresponding capacitors to their minimum or maximum values. To eliminate the impact from the Load branch, the measurements were performed at the output port of the MFMB with the input port shorted. As an example, the result corresponding to the tuning of C_{T1} is presented in Fig. 4. Here, we define $X_{tune,1}$, $X_{tune,2}$, and $X_{tune,3}$ as the reactance corresponding to the excitation frequencies at 13.56, 27.12, and 40.68 MHz, respectively. As one can see in Fig. 4(a), decreasing values of C_{T1} lead to an increase of the resonant frequency in the range close to 13.56 MHz (indicated by a gray arrow). Consequently, $X_{tune,1}$ at 13.56 MHz varies from 44 to 62 Ω, as more clearly shown in Fig. 4(b). This limited variation of $X_{tune,1}$ is due to the lower and upper limits of the range of C_{T1}. Although sufficient for the reactor under study, a larger $X_{tune,1}$ variation range could be achieved with a larger capacitance range, increasing the flexibility of the design.

This measurement gives a first indicative result concerning the independence of the matching at each frequency. One would desire that changing the impedance at one harmonic (in this case, 13.56 MHz) has little impact on the impedance at other harmonics. One can see that it is the case in Fig. 4, wherein the tuning of C_{T1} causes almost no change at 27.12 and 40.68 MHz. This is not the case in general, however, so the impact of such "cross-talk" (or lack thereof) between the matching at adjacent harmonics will be quantified in more depth in Sec. III C.

Analogous to the measurements in Fig. 4, the ranges of $X_{tune,2}$ and $X_{tune,3}$ were also characterized. A summary of these results are shown in Table I. One can see that for the measurements of this experiment, the range of values obtainable at 13.56 MHz (through the adjustment of C_{T1}) is quite limited, compared to those at the higher harmonics (obtained by adjusting C_{T2} and C_{T3}).

In an analogous fashion, the range of imaginary admittance values (susceptance, B) at each of the three harmonics ($B_{load,i}$) accessible by tuning the three Load capacitors was measured. As was done for the Tune branch measurements described in Sec. III A, the characterization of each $B_{load,i}$ was made with the resonant frequencies of the other two sub-branches set as far as possible away. To minimize the impact from the Tune branch, the measurements were made at the input port of the MFMB with the output port open. The results are shown in Table II, presented as both the negative range of values and a positive range.

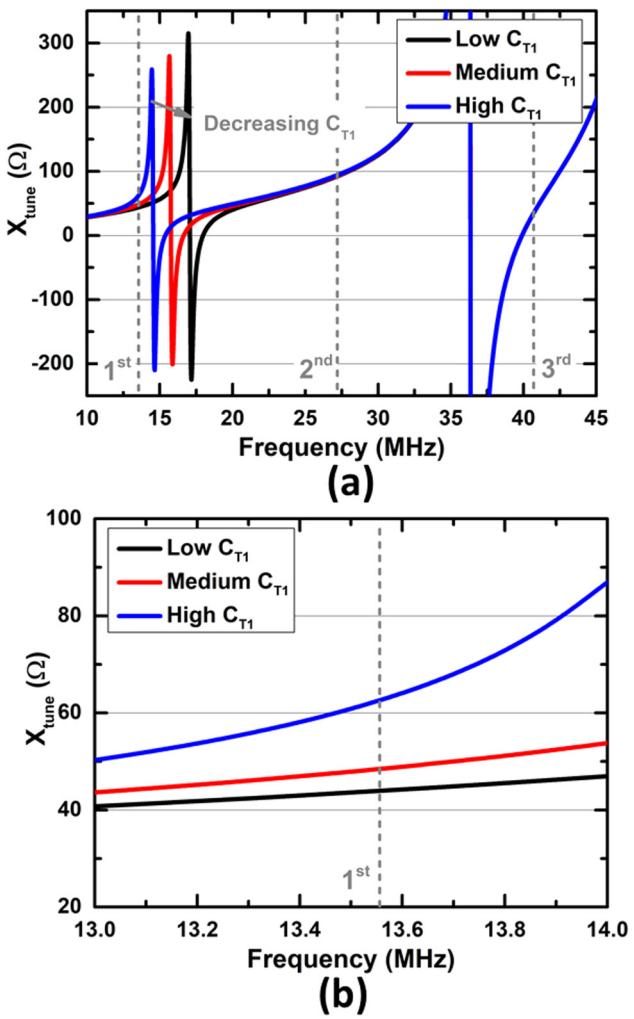

FIG. 4. Tune branch reactance X_{tune} for frequencies in the range of (a) 10–45 MHz and (b) 13–14 MHz when setting C_{T1} at low, medium, and high values (order indicated in figure). The gray dashed lines indicate the excitation frequencies at 13.56 MHz (first), 27.12 MHz (second), and 40.68 MHz (third).

B. Range of load impedance for which perfect, single-frequency matching is achievable

Knowing the ranges of the Tune reactance and Load susceptance that are accessible when tuning the capacitors intended for each frequency, we can make a first estimation of the range of plasma system impedances (including reactor and cable) that can be matched at each harmonic. One should note that in doing so, we continue to neglect the real parts of the Tune impedance and the Load admittance (which would induce significant losses). The justification for this is that, in principle, these losses can be minimized through engineering (better materials and component design), although this remains to be demonstrated.

The two necessary conditions for achieving optimal impedance matching, i.e., maximal power transfer to the plasma reactor system, are (i) the real part of the final load impedance, R_L, must be equal to 50 Ω (the characteristic impedance of the cable) and (ii) the imaginary part must be equal to 0 Ω. For the MFMB design under study, one can consider the necessary impedance transformation in several steps. Denoting the original plasma impedance (including all cable and chamber effects) as $Z_{pl,i} = R_{pl,i} + iX_{pl,i}$, the resulting load impedance

TABLE I. Range of accessible Tune branch reactances, $X_{tune,i}$, at each harmonic frequency.

Frequency	13.56 MHz	27.12 MHz	40.68 MHz
$X_{tune,i}$ (Ω)	44 to 62	−1722 to 1665	−763 to 1017

TABLE II. Range of accessible Load branch susceptance, $B_{load,i}$, at each harmonic frequency.

Frequency	13.56 MHz	27.12 MHz	40.68 MHz
$B_{load,i}$ (S)	−1.05 to −0.037, 0.009 to 1.09	−0.014 to −1.12, 0.006 to 1.16	−0.79 to −0.025, 0.001 to 0.81

TABLE III. Range of the real part of the plasma load, $R_{pl,i}$, that can be corrected and matched by the "Load" branch.

Frequency	13.56 MHz	27.12 MHz	40.68 MHz
$R_{pl,i}$ (Ω)	0.02 to 41.8	0.01 to 45.8	0.03 to 49.9

after the impedance modification through the Tune branch (having a reactance of $X_{tune,i}$) can be expressed as

$$Z_{pl+tune,i} = R_{pl,i} + iX_{pl,i} + iX_{tune,i} = R_{pl,i} + iX_{pl+tune,i}. \quad (3)$$

Since the "Load" branch is parallel-connected, we must modify Eq. (3) to be an admittance. This leads to

$$Y_{pl+tune,i} = \frac{R_{pl,i}}{R_{pl,i}^2 + X_{pl+tune,i}^2} - i\frac{X_{pl+tune,i}}{R_{pl,i}^2 + X_{pl+tune,i}^2}. \quad (4)$$

Adding the "Load" branch in parallel to this admittance serves to cancel out the imaginary part of $Y_{pl+tune,i}$ (namely, the susceptance, B), leaving only the conductance, G_L, which must be equal to $1/R_L = 0.02$ S. Mathematically, the "Target" final load admittance $Y_{target,i}$ after both branches should be as follows:

$$Y_{target,i} = Y_{pl+tune,i} + iB_{load,i} = G_L. \quad (5)$$

By combining Eqs. (4) and (5), the "Target" load reactance $X_{target,i}$ after adding the reactance of the "Tune" branch can be expressed as

$$X_{target,i} = X_{pl+tune,i} = \pm\sqrt{R_L R_{pl,i} - R_{pl,i}^2}. \quad (6)$$

In analogy, the desired susceptance of the "Load" branch can be calculated as

$$B_{load,i} = \frac{\pm\sqrt{R_L R_{pl,i} - R_{pl,i}^2}}{R_L R_{pl,i}}. \quad (7)$$

Here, we will only focus on the case with a positive solution to Eqs. (6) and (7), although a similar analysis can be made when the negative solution is considered. One can notice that the required value of $B_{load,i}$ is fully determined by the plasma resistance. Conversely, knowing the range of $B_{load,i}$ accessible by the Load branch allows one to estimate the range of plasma resistances that could satisfy this condition. By transforming Eq. (7), one obtains

$$R_{pl,i} = \frac{R_L}{R_L^2 B_{load,i}^2 + 1}. \quad (8)$$

Using Eq. (8) and the accessible range of $B_{load,i}$ determined in Sec. III A, we can therefore express the range of plasma resistances at each harmonic that can be independently matched. (In doing so, we are implicitly minimizing the impact of the other resonant circuits by tuning them to be as far as possible from the harmonic in question, as was done in Sec. III A.) The results are shown in Table III, showing the large range of the real part of the plasma load at each frequency, $R_{pl,i}$, that can be independently matched by this MFMB circuit.

It may also be noted that a real solution for both Eqs. (6) and (7) exists only when $R_{pl,i} < 50\,\Omega$. For the case of $R_{pl,i} > 50\,\Omega$, an analogous method may be used by first placing another set of resonant circuits in parallel with the plasma load, and then the Tune branch and Load branch as used in the MFMB under study, as suggested in Ref. 34. However, this configuration is not examined in more depth in this paper.

Having addressed the range of plasma resistances that can be corrected by the Load branch, we must now determine the range of plasma reactances that can be corrected by the Tune branch. As an example, we address the impedance matching at 13.56 MHz and refer to the Smith chart in Fig. 5, wherein the impedance is normalized to the value of R_L, 50 Ω. By adding the reactance of the Tune branch, the plasma load impedance is moved along the constant-resistance circles of the Smith chart.[35] As one can see in Fig. 5, the solid curved arrows depict several examples of reactance paths on different constant-resistance circles. For perfect matching to be possible, the sum of the plasma (system) impedance and the Tune branch impedance, $R_{pl,i} + iX_{pl+tune,i}$, must terminate on the "Target" reactance semicircle (solid), which corresponds to a circle of constant conductance (noted as a dashed line in the admittance view of the Smith chart). This limits the range of possible plasma resistance/reactance sets that can be matched by this MFMB, due to the limited range of the Tune branch. At 13.56 MHz, values of $X_{tune,1}$ from 44 to 62 Ω were achievable, meaning that initial plasma impedances must lie in the outlined gray zone in Fig. 5 to be able to achieve perfect matching.

Furthermore, one must further limit the gray zone in Fig. 5 to a range of values of plasma resistance, due to the limited range of load resistances $R_{pl,1}$ that can be addressed by the Load branch, as listed in Table III. However, this limitation has a much lesser impact at 13.56 MHz, as the matchable values of plasma resistance ranged from 0.02 to 41.8 Ω.

Analogously, the range of values of $Z_{pl,2}$ and $Z_{pl,3}$ that can be matched were also determined and are shown in Figs. 6 and 7, respectively. As one can see, for 27.12 and 40.68 MHz, the values of $Z_{pl,2}$ and $Z_{pl,3}$ for which perfect matching could be obtained both cover a much larger range than that for 13.56 MHz. This is directly attributable to the much larger range of $X_{tune,i}$ at these higher harmonics (Table I) which could in future be resolved by the use of a variable capacitor for C_{T1} with a larger tuning range.

Although useful as a first estimation, the above results do not address the desired utilization of this MFMB, which is simultaneous impedance matching at all three frequencies. However, given all the degrees of freedom of the matchbox

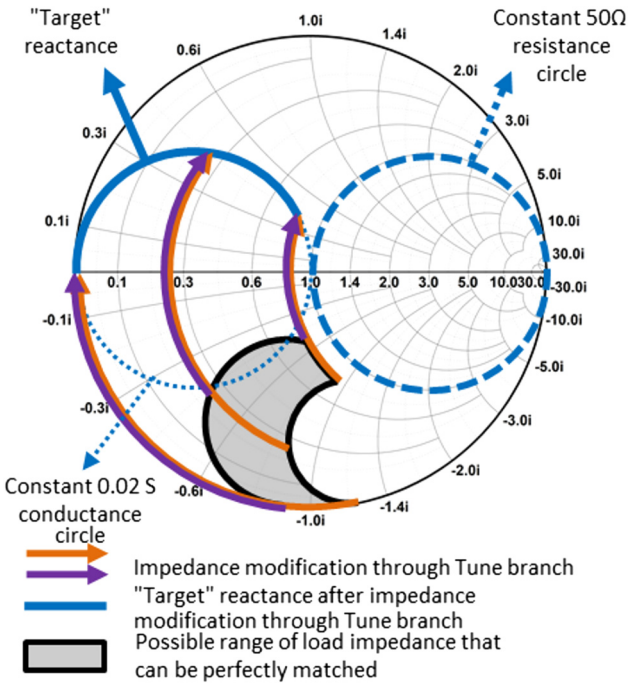

FIG. 5. Possible range of load impedance $Z_{pl,1}$ (normalized to 50 Ω) at 13.56 MHz that can be perfectly matched.

(six adjustable capacitors for the three harmonics), manually determining the set of simultaneously matchable impedances is an impossible task on a human time scale. (For a conservative set of 100 settings per capacitor, $\sim 10^{12}$ measurements would have to be obtained.) In Sec. III C, we instead present

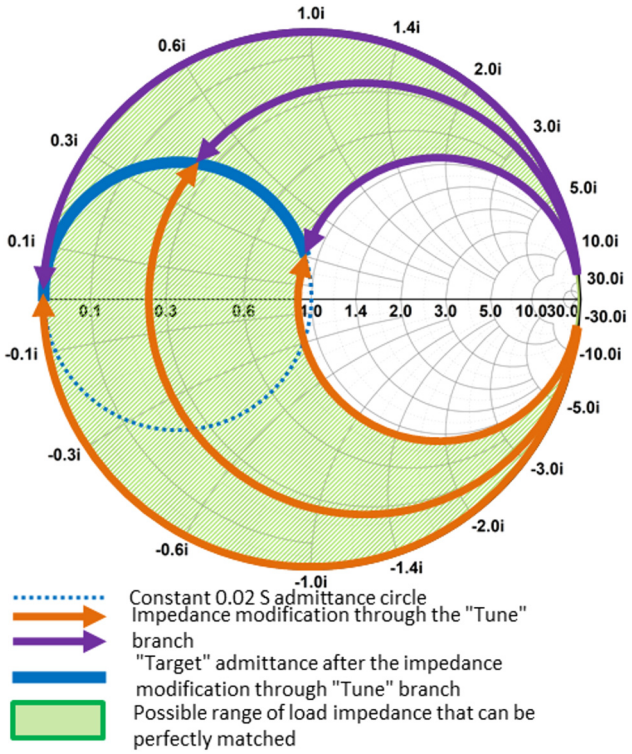

FIG. 6. Range of load impedances $Z_{pl,2}$ (normalized to 50 Ω) at 27.12 MHz that can be perfectly matched.

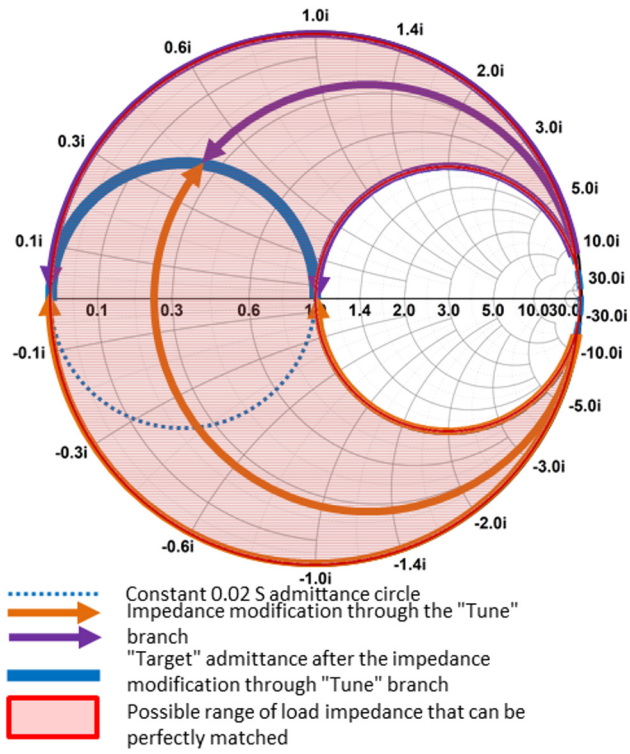

FIG. 7. Range of load impedances $Z_{pl,3}$ (normalized to 50 Ω) at 40.68 MHz that can be perfectly matched.

an analysis of the independence of the matching at each frequency when simultaneous, three-frequency matching is performed on a reasonable model circuit.

The second weakness of this first estimation is that the ranges presented do not take into account the resistive losses in the real LC circuits, including the circuits in the other subbranches. The impact of these parasitic resistances will also change according to the load impedance and can impact how much power is transferred to the load versus absorbed within the matchbox (even when no reflected power is observed from the matchbox input). These effects will be addressed in practice in Sec. IV, when the MFMB is used to match to an ignited plasma system.

Nevertheless, the procedure followed in this section and the mapping performed offer insights into the range of load impedances for which a given MFMB design might ideally achieve perfect matching.

C. Independence of matching: Sensitivity to changes at adjoining harmonics

A defining characteristic of this MFMB concept is the possibility of achieving simultaneous and independent matching at each harmonic, that is, to be able to adjust the matching at one harmonic without affecting that at the others. However, quantifying this property generically for all possible matching conditions is not a tractable task. We have therefore attempted to quantify the independence of matching for different harmonics for a few example models of reactor impedances.

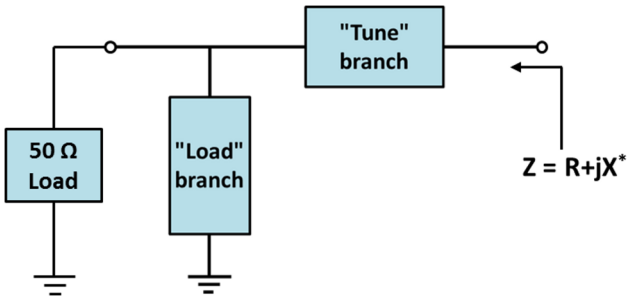

FIG. 8. Diagram showing the conjugate matching technique.

The determination of the matched impedance was done using the conjugate matching technique, as shown in Fig. 8. In this technique, a 50 Ω load is attached at the input of the matchbox, and the impedance that appears at the output is the complex conjugate of the impedance of the load that would be matched for those matchbox settings.

Using this configuration, two representative plasma loads were chosen, in the form of two resistor–capacitor pair: (5 Ω, 300 pF) and (3 Ω, 200 pF). For each of these loads, a "Target" conjugate impedance at each of the three harmonics (13.56, 27.12, and 40.68 MHz) can be calculated, and the six matchbox capacitors were set to simultaneously obtain matching at all three harmonics.

To quantify the sensitivity of the matching to changes at adjoining frequencies, the following procedure was then performed. The reactance of the matched impedance at a given harmonic was changed, keeping the matched resistance at that harmonic the same. For example, to change the matched impedance at 13.56 MHz, capacitors C_{T1} and C_{L1} were adjusted. The resulting matched impedance at the adjoining harmonic (in this case, 27.12 MHz) was then measured, without changing the position of any other capacitors. This was repeated, changing the reactance at the original harmonic by a factor ranging from as low as

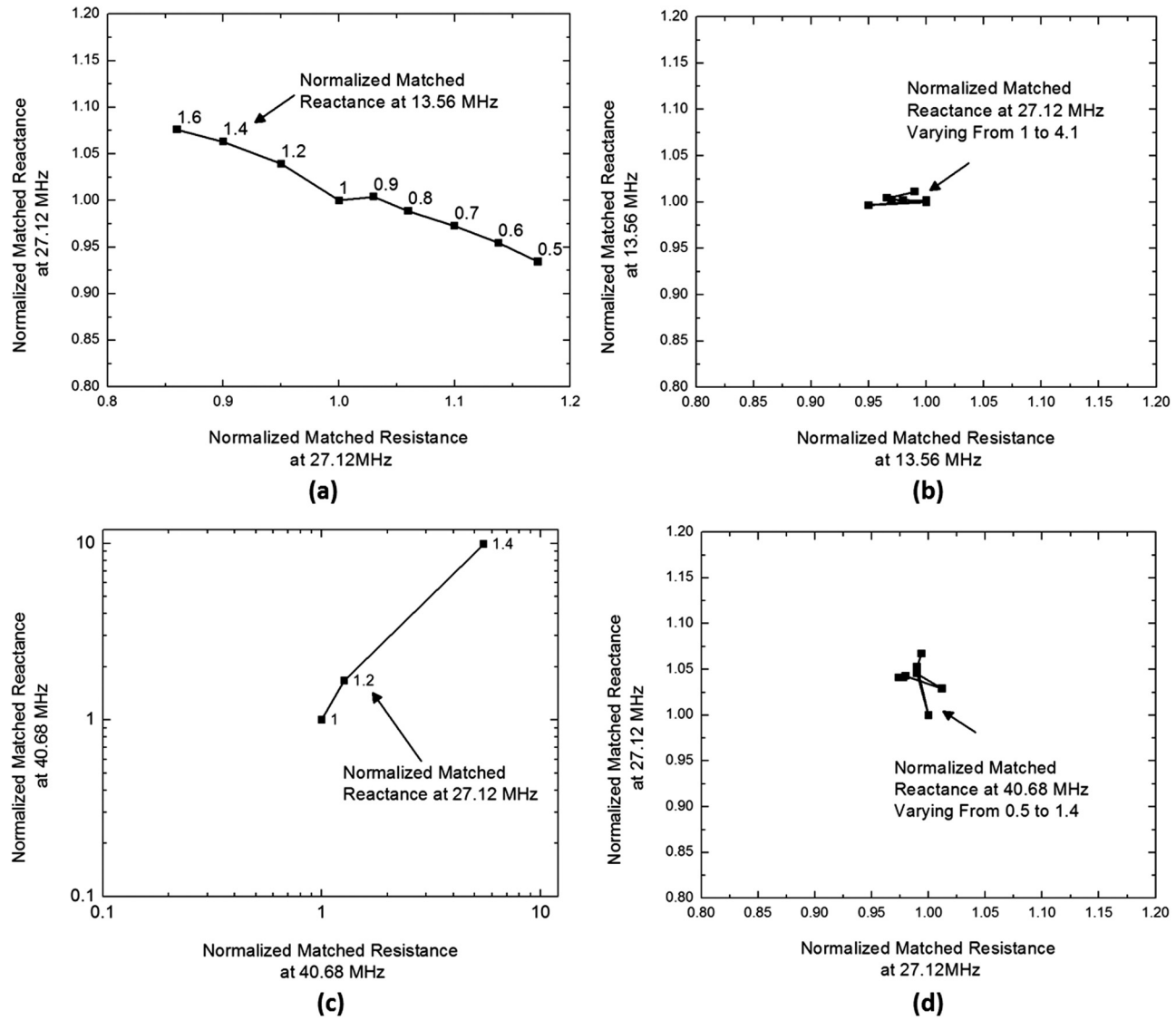

FIG. 9. Parametric plots showing changes in matched impedance at adjacent harmonic when matching adjusted at initial harmonic. Circuit model uses components with values of (5 Ω, 300 pF). Response (a) at 27.12 MHz for adjustments at 13.56 MHz, (b) at 13.56 MHz for adjustments at 27.12 MHz, (c) at 40.68 MHz for adjustments at 27.12 MHz, and (d) at 27.12 MHz for adjustments at 40.68 MHz. Notice logarithmic scale in Fig. 9(c).

0.5 to 2 or higher (depending on the range of the variable capacitors).

The results of these measurements are presented in Figs. 9 and 10 as parametric plots, for the resistor–capacitor pairs of (5 Ω, 300 pF) and (3 Ω, 200 pF), respectively. Most data are presented on a scale representing a ±20% change in the resistance and reactance at the adjacent harmonic, unless highlighted otherwise. What can be immediately noted in these figures is that the level of sensitivity changes according to the pairs of harmonics interacting. In Figs. 9(b) and 9(d), it is shown that adjusting the matching at the higher harmonic had a negligible impact at the lower harmonic. The inverse was not true, however. Figure 9(c) shows that the match at 40.68 MHz was very sensitive to changes concerning 27.12 MHz (note the logarithmic scale), and Fig. 9(a) demonstrates a strong impact on the matched resistance at 27.12 MHz and much less on the matched reactance (always less than 20% though).

Figure 10 underlines the fact that this sensitivity will depend on the load impedance. Figures 10(b)–10(d) show measurable sensitivities to changes at adjacent harmonics (although all still less than 20%), and Fig. 10(a) again requires a change in scale to show the data, as the halving of the matched reactance at 13.56 MHz causes a 40% increase in the matched reactance at 27.12 MHz.

One trend that is supported by the data in Figs. 9 and 10 is that the impact on matching is strongest when the frequency being tuned is the lower one and the one being impacted is the higher. This suggests that the algorithm used to find simultaneous matching conditions should focus on the lower frequencies first, then fine tune for higher ones.

IV. IMPEDANCE MATCHING TO AN AR PLASMA

The final study of this work explored the application of the MFMB to match power to a low-pressure plasma reactor

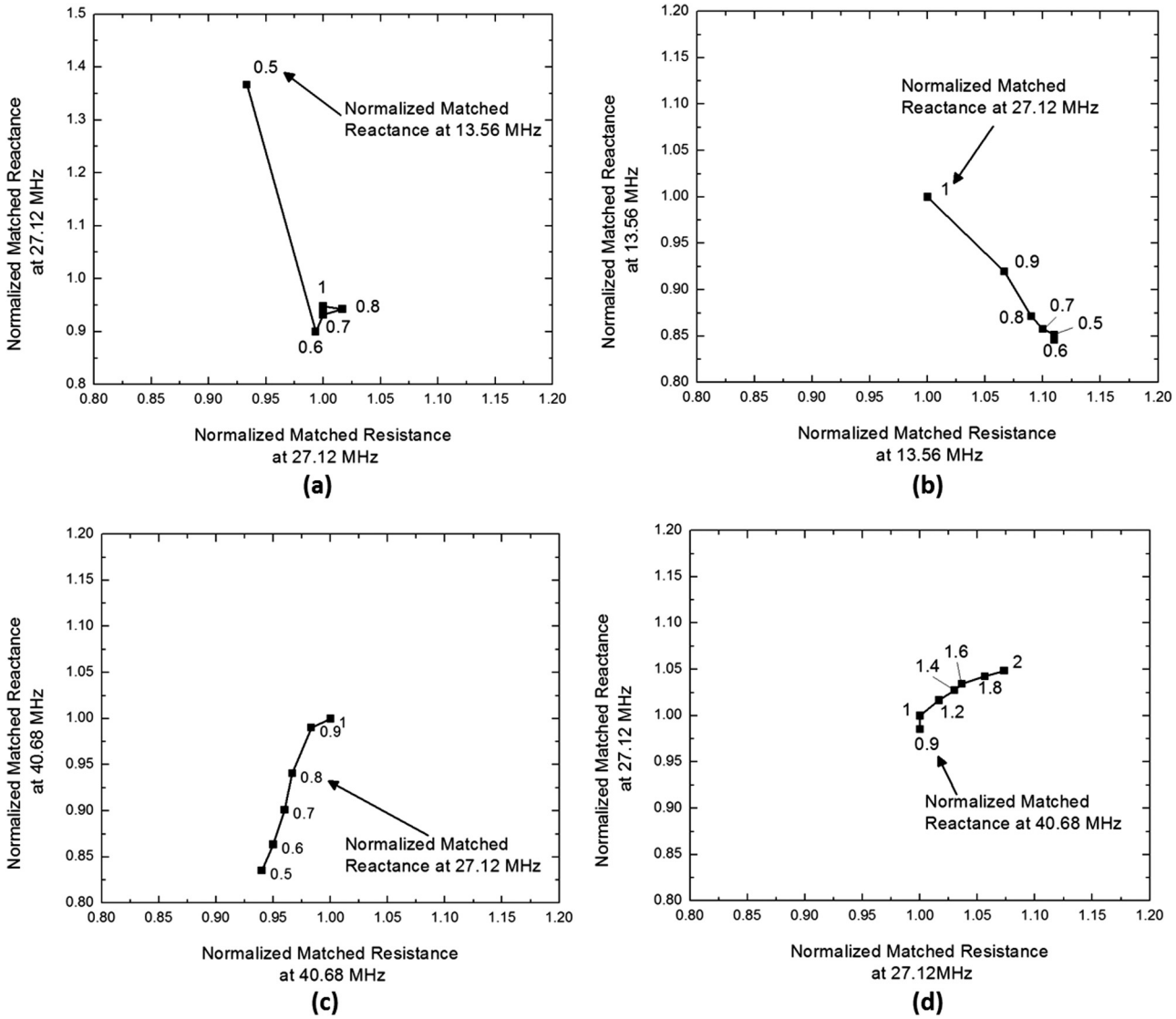

FIG. 10. Parametric plots showing changes in matched impedance at adjacent harmonic when matching adjusted at initial harmonic. Circuit model uses components with values of (3 Ω, 200 pF). Response (a) at 27.12 MHz for adjustments at 13.56 MHz, (b) at 13.56 MHz for adjustments at 27.12 MHz, (c) at 40.68 MHz for adjustments at 27.12 MHz, and (d) at 27.12 MHz for adjustments at 40.68 MHz. Notice different scale in Fig. 10(a).

chamber with a plasma ignited. Measurements were made on an Argon plasma at 200 mTorr. The open symbols in the Smith chart in Fig. 11 show the plasma reactor impedance at each frequency (measured at the output of the MFMB, including the 6.7-m coupling cable, Probe Position II). The matchable ranges of the load impedance for each frequency are also depicted (shaded areas). To achieve the optimum impedance matching, the capacitance values were adjusted as follows: $C_{T1} = 1335$ pF, $C_{T2} = 685$ pF, $C_{T3} = 425$ pF, $C_{L1} = 127$ pF, $C_{L2} = 220$ pF, and $C_{L3} = 137$ pF. The final load impedance at each frequency after impedance matching as seen by the RF source (Probe Position I) is also shown (solid symbols).

As one can see in the Smith chart in Fig. 11, through the impedance transformation, the final load impedance at each frequency is much closer to 50 Ω (the origin point) than without impedance matching. From these points, the power reflection coefficient Γ_i and thus the power coupling efficiency k_i (at the matchbox input) can be estimated based on Eq. (2). This can be compared to the same measurement, with the same output voltage from the AWG to the amplifier (110 mV), but performed without the MFMB in place (although the 6.7 m cable was still present). As one can see in Fig. 12(a), this MFMB circuit gives almost perfect power coupling at 13.56 and 27.12 MHz (right bars), compared to less than 40% without matching (left, black bars). At 40.68 MHz, the matching and power coupling (~80%) is less perfect, although still a significant improvement on no matching.

The calculation of power coupling in this case does not take into account losses in the matchbox. As a demonstration of improved power coupling to the plasma chamber, a second measurement was performed wherein the output voltage from the AWG was kept at 110 mV and the power coupled to the plasma system was measured. As shown in Fig. 12(b), the coupled powers at each frequency are all significantly higher when impedance matching is used. This leads to a total coupled power $P_{w,total}$ of ~24.2 W (with a peak–peak voltage on the electrode V_{pp} of 73.0 V, as shown in Table III), compared to a value of ~7.5 W (with a V_{pp} of 45.0 V) without matching.

However, a careful reader may note that the plasma impedance at 13.56 MHz actually lies *outside* the estimated

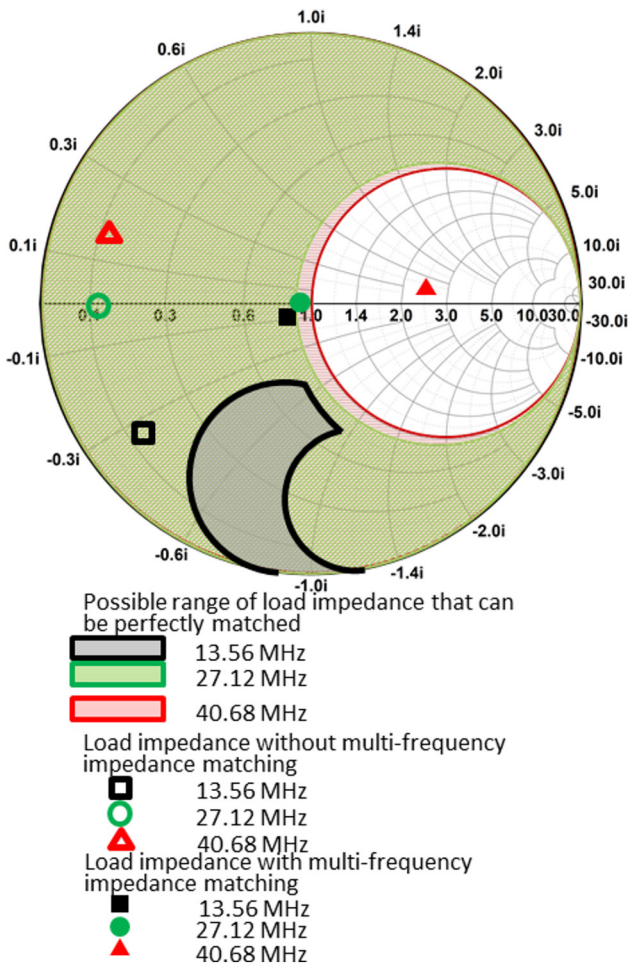

FIG. 11. Load impedance at each frequency, measured at the input of the MFMB (Position I, closed symbols) and at the output of the MFMB (Position II, filled symbols). The shaded areas depict the possible ranges of the load impedance that can be perfectly matched by the MFMB under study.

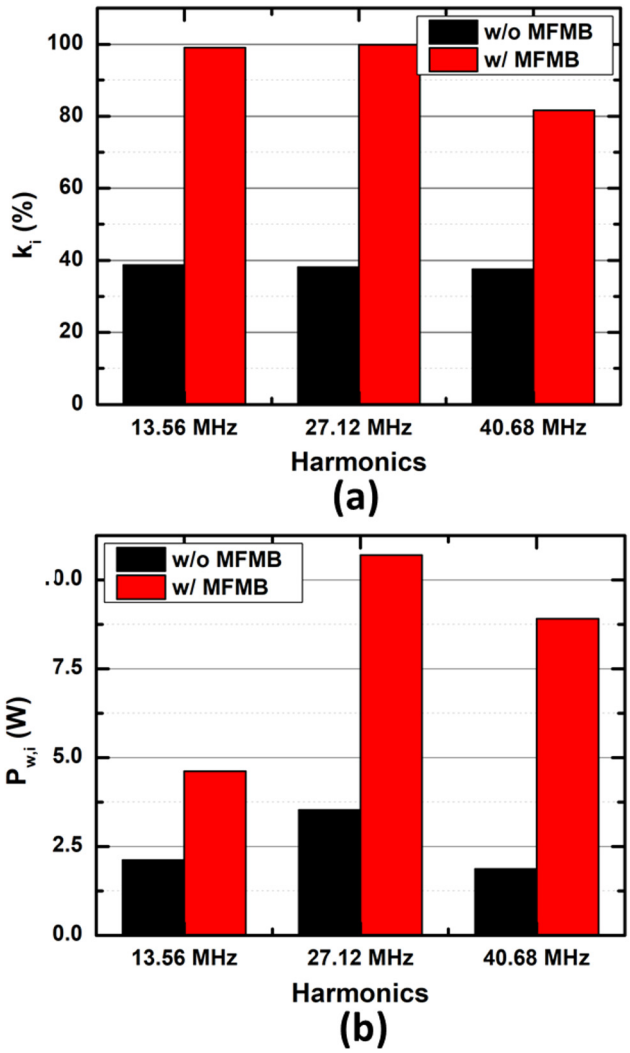

FIG. 12. (a) Power coupling efficiency k_i and (b) coupled power $P_{w,i}$ at each frequency for the Ar plasma load with (right) and without (left) using MFMB matching.

TABLE IV. Comparison of the power coupling efficiency at each frequency k_i and the total coupled power $P_{w,total}$ for the Ar plasma with and without using the MFMB. V_{pp} represents the peak–peak voltage on the electrode.

		Without MFMB					With MFMB				
V_{awg} (mV)	P_r (mTorr)	$P_{w,total}$ (W)	V_{pp} (V)	k_1 (%)	k_2 (%)	k_3 (%)	$P_{w,total}$ (W)	V_{pp} (V)	k_1 (%)	k_2 (%)	k_3 (%)
110	200	7.5	45.0	38.7	38.1	37.5	24.2	73.0	99.1	99.9	81.6
	300	7.8	44.5	39.9	38.8	38.1	24.5	59.5	99.8	99.8	83.4
170	200	13.1	52.0	31.6	30.6	30.0	50.0	81.0	99.8	99.4	78.1
	300	13.6	52.0	32.9	31.5	30.8	51.8	75.0	99.8	98.5	81.0

range of load impedances addressable by the MFMB, while a k_1 of ~99% was in reality obtained. Moreover, the initial load impedance at 40.68 MHz is located well *inside* of the corresponding possible range for maximal power transfer, while a k_3 of only ~80% was obtained. This discrepancy is a natural product of the limitations of the characterization performed, which first treated each harmonic separately, and second ignored parasitic absorption in the matchbox. The cross-talk between harmonics demonstrated in Sec. III C and the presence of parasitic absorption cannot be neglected in practical operation and outlines the limits of the single-frequency characterization.

Measurements were also made for other plasma conditions with different values of gas pressure and power. The results are summarized in Table IV. As one can see, for all the studied scenarios, the power coupling is significantly increased at all frequencies.

It is also worth noting that the power coupling measurements were performed in both cases by placing the VI probe at the output of the amplifier, and measurements therefore include the effect of losses in both the cable (for the unmatched case) and the MFMB plus the cable (for the matched case). The actual power delivered to the plasma reactor (or the true power coupling efficiency to the plasma) will be lower than the values presented above, since some of the coupled power will be dissipated in the coaxial coupling cable and the MFMB itself (when present). Therefore, the true utility of this MFMB design will be most apparent through the use of a less lossy coupling cable and better passive components in the MFMB. Nevertheless, the practical effectiveness of the MFMB is clearly demonstrated through the increased voltage at the electrode for the same voltage at the input of the amplifier.

V. CONCLUSION

A simple, broadband multifrequency matchbox has been constructed for the impedance matching of a three-harmonic tailored voltage waveform excitation source to a plasma load. This novel matchbox is derived from a classical "L-type" matching network but with the usual single L and C components replaced by multiple LC resonant circuits excited near their resonance frequencies. For each branch, the number of LC resonant circuits must be equal to the number of excitation frequencies. At first, the analytical treatment of the system considered the system as three simple "L-type" matchboxes each performing the impedance matching at a single frequency and quantified the idealized matching that could be achieved independently at each frequency. A further analysis quantified the impact of matched impedance changes on the adjoining harmonic and found that the impact was weaker on lower frequencies when adjusting higher ones, than the inverse. The system was then characterized experimentally for a three-harmonic (fundamental frequency at 13.56 MHz) excited Ar plasma operated over a range of gas pressures and coupled powers. For all the studied scenarios, the power coupling efficiency to the plasma system was significantly increased through the use of the multifrequency matchbox. Up to 99% power coupling efficiency was observed at 13.56 and 27.12 MHz, and of the order of 80% was achieved for 40.68 MHz. Such promising preliminary results prove the functionality of the multifrequency matchbox, indicating that it is a promising solution for the practical application of the tailored voltage waveform technique in industrially relevant plasma processes.

ACKNOWLEDGMENTS

The work presented herein was funded by Université Paris-Saclay through the "SERPICO" project in the AAP "Prematuration IDEX PIA-ANR" 2017 program and by the Essonne Department of France through the "ASTRE—NanoShaper" project.

[1]A. Perret, P. Chabert, J. Jolly, and J.-P. Booth, Appl. Phys. Lett. **86**, 021501 (2005).
[2]H. Goto, M. Sasaki, T. Ohmi, T. Shibata, A. Yamagami, N. Okamura, and O. Kamiya, Jpn. J. Appl. Phys. **29**, L2395 (1990).
[3]M. M. Turner and P. Chabert, Phys. Rev. Lett. **96**, 205001 (2006).
[4]A. Derzsi, Z. Donkó, and J. Schulze, J. Phys. Appl. Phys. **46**, 482001 (2013).
[5]D. O'Connell, T. Gans, E. Semmler, and P. Awakowicz, Appl. Phys. Lett. **93**, 081502 (2008).
[6]J. P. Booth, G. Curley, D. Marić, and P. Chabert, Plasma Sources Sci. Technol. **19**, 015005 (2010).
[7]Z. Donko, J. Schulze, P. Hartmann, I. Korolov, U. Czarnetzki, and E. Schungel, Appl. Phys. Lett. **97**, 81501 (2010).
[8]B. G. Heil, U. Czarnetzki, R. P. Brinkmann, and T. Mussenbrock, J. Phys. Appl. Phys. **41**, 165202 (2008).
[9]Z. Donkó, J. Schulze, B. G. Heil, and U. Czarnetzki, J. Phys. Appl. Phys. **42**, 025205 (2009).
[10]B. G. Heil, R. P. Brinkmann, and U. Czarnetzki, J. Phys. Appl. Phys. **41**, 225208 (2008).

[11]J. Schulze, E. Schüngel, and U. Czarnetzki, J. Phys. Appl. Phys. **42**, 092005 (2009).
[12]B. Bruneau, T. Novikova, T. Lafleur, J.-P. Booth, and E. V. Johnson, Plasma Sources Sci. Technol. **23**, 065010 (2014).
[13]B. Bruneau, T. Gans, D. O'Connell, A. Greb, E. V. Johnson, and J.-P. Booth, Phys. Rev. Lett. **114**, 125002 (2015).
[14]J. Schulze, E. Schüngel, U. Czarnetzki, M. Gebhardt, R. P. Brinkmann, and T. Mussenbrock, Appl. Phys. Lett. **98**, 031501 (2011).
[15]T. Lafleur, Plasma Sources Sci. Technol. **25**, 013001 (2016).
[16]B. Bruneau, R. Cariou, J.-C. Dornstetter, M. Lepecq, J.-L. Maurice, P. Roca i Cabarrocas, and E. V. Johnson, IEEE J. Photovolt. **4**, 1361 (2014).
[17]E. V. Johnson, T. Verbeke, J.-C. Vanel, and J.-P. Booth, J. Phys. Appl. Phys. **43**, 412001 (2010).
[18]D. Hrunski *et al.*, Vacuum **87**, 114 (2013).
[19]B. Bruneau, J. K. Wang, J.-C. Dornstetter, and E. V. Johnson, J. Appl. Phys. **115**, 084901 (2014).
[20]E. Schüngel, R. Hofmann, S. Mohr, J. Schulze, J. Röpcke, and U. Czarnetzki, Thin Solid Films **574**, 60 (2015).
[21]Y. Zhang, M. J. Kushner, S. Sriraman, A. Marakhtanov, J. Holland, and A. Paterson, J. Vac. Sci. Technol. A **33**, 031302 (2015).
[22]G. Fischer, E. Drahi, F. Lebreton, P. Bulkin, G. Poulain, and E. V. Johnson, 33rd European Photovoltaic Solar Energy Conference and Exhibition, Amsterdam, 25–29 September 2017.
[23]J. K. Wang, C. Longeaud, F. Ventosinos, D. Daineka, M. E. Yaakoubi, and E. V. Johnson, Phys. Status Solidi C **13**, 735 (2016).
[24]J. K. Wang and E. V. Johnson, Plasma Sources Sci. Technol. **26**, 01LT01 (2017).
[25]D. Hrunski, A. Janssen, T. Fritz, T. Hegemann, C. Clark, U. Schreiber, and G. Grabosch, Thin Solid Films **532**, 56 (2013).
[26]T. Lafleur, P. A. Delattre, J.-P. Booth, E. V. Johnson, and S. Dine, Rev. Sci. Instrum. **84**, 015001 (2013).
[27]J. Franek, S. Brandt, B. Berger, M. Liese, M. Barthel, E. Schüngel, and J. Schulze, Rev. Sci. Instrum. **86**, 053504 (2015).
[28]E. V. Johnson and J.-P. Booth, WO2018087189 (A1) (17 May 2018).
[29]F. Schmidt, J. Schulze, E. Johnson, J.-P. Booth, D. Keil, D. M. French, J. Trieschmann, and T. Mussenbrock, Plasma Sources Sci. Technol. **27**, 095012 (2018).
[30]T. Lafleur, P. A. Delattre, E. V. Johnson, and J. P. Booth, Plasma Phys. Control. Fusion **55**, 124002 (2013).
[31]G. Fischer, K. Ouaras, E. Drahi, B. Bruneau, and E. V. Johnson, Plasma Sources Sci. Technol. **27**, 074003 (2018).
[32]S.-B. Wang and A. E. Wendt, J. Appl. Phys. **88**, 643 (2000).
[33]M. M. Patterson, H.-Y. Chu, and A. E. Wendt, Plasma Sources Sci. Technol. **16**, 257 (2007).
[34]E. V. Johnson and J.-P. Booth, EP2675064A1 (18 December 2013).
[35]P. H. Smith, *Electronic Applications of the Smith Chart: In Waveguide, Circuit, and Component Analysis* (New York, McGraw-Hill, 1969).